nuclear fusion
IAEA

PAPER • OPEN ACCESS

Deuterium retention in cold spray tantalum coatings vs. polycrystalline tungsten and tantalum

To cite this article: Mykola Ialovega *et al* 2025 *Nucl. Fusion* **65** 076042

View the article online for updates and enhancements.

You may also like

- Mitigation of ICRF—edge plasma interaction in Alcator C-Mod
R. Diab, S.G. Baek, A.Q. Kuang et al.
- Low collisionality, peeling limited pedestals in JET-ILW: effect of density and isotope mass on pedestal structure, pedestal stability and pedestal prediction in deuterium and mixed deuterium/tritium plasmas
L. Frassinetti, D. King, S. Saarelma et al.
- Integrated modeling of RF-induced tungsten erosion at ICRH antenna structures in the WEST tokamak
A. Kumar, W. Tierens, T. Younkin et al.

This content was downloaded from IP address 134.94.123.71 on 06/03/2026 at 08:43

OPEN ACCESS
IOP Publishing | International Atomic Energy Agency
Nuclear Fusion
Nucl. Fusion **65** (2025) 076042 (11pp)
https://doi.org/10.1088/1741-4326/ade4d7

Deuterium retention in cold spray tantalum coatings vs. polycrystalline tungsten and tantalum

Mykola Ialovega[1,2,3,*], Marcos Xavier Navarro-Gonzalez[1], Régis Bisson[2], Jay Anderson[3], Thierry Angot[2], Tyler Dabney[1], Cary Forest[3], Arkadi Kreter[4], Danah Velez[1], Evan Willing[1], Hwasung Yeom[5], Kumar Sridharan[1] and Oliver Schmitz[1]

[1] Department of Nuclear Engineering and Engineering Physics, University of Wisconsin-Madison, 1500 Engineering Drive, Madison, WI 53706, United States of America
[2] Aix Marseille Univ., CNRS, PIIM, UMR 7345, 13013 Marseille, France
[3] Department of Physics, University of Wisconsin-Madison, 1150 University Ave., Madison, WI 53706, United States of America
[4] Forschungszentrum Jülich GmbH, IEK-4, 52425 Jülich, Germany
[5] Division of Advanced Nuclear Engineering, Pohang University of Science and Technology (POSTECH), Pohang 37673, Korea, Republic Of

E-mail: ialovega@wisc.edu

Received 15 January 2024, revised 13 May 2025
Accepted for publication 16 June 2025
Published 27 June 2025

Abstract

Enhanced deuterium retention in tantalum (Ta) cold spray coatings, compared to reference polycrystalline tantalum and tungsten materials, has been evaluated using the thermal desorption spectrometry technique. Tantalum coatings, deposited via cold spray technology on 316L stainless steel substrates, are proposed as plasma-facing material surfaces with hydrogen gettering functionality for advanced fusion concepts. The materials were exposed to 95 eV D ions at a flux of 1.6–3.5 $\times$ 10^{21} D m^{-2} s^{-1}. Retention was measured as a function of incident ion fluence and surface temperature. The results highlight an increased deuterium inventory in Ta cold spray coatings by a factor of 3.5 compared to polycrystalline tantalum and by two orders of magnitude compared to polycrystalline tungsten. A tendency for retention saturation in tantalum is observed at a fluence above 1 $\times$ 10^{24} D m^{-2}. While deuterium retention gradually decreases with increasing surface temperature from 400 K to 925 K for polycrystalline tungsten, it remains constant for polycrystalline tantalum. In contrast, retention in Ta coatings significantly decreases when the surface temperature exceeds 750 K. The microstructure of the cold spray Ta coatings plays a crucial role in the dynamics of deuterium trapping and release. Tantalum also exhibits a superior resistance to blister formation compared to tungsten when subjected to a high dose of deuterium.

Keywords: tantalum, tungsten, cold spray deposition, hydrogen isotopes, retention, thermal desorption, blisters

(Some figures may appear in colour only in the online journal)

* Author to whom any correspondence should be addressed.

Original Content from this work may be used under the terms of the Creative Commons Attribution 4.0 licence. Any further distribution of this work must maintain attribution to the author(s) and the title of the work, journal citation and DOI.

 © 2025 The Author(s). Published by IOP Publishing Ltd on behalf of the IAEA

1. Introduction

Tantalum (Ta) is a promising candidate material for the first-wall gettering interface in advanced fusion concepts due to its high melting point, good thermal conductivity, resistance to sputtering, excellent room-temperature ductility, and unique corrosion resistance [1]. Moreover, Ta exhibits exothermic hydrogen absorption, which results in a significantly higher inventory of hydrogen isotopes (HIs) compared to tungsten (W), a commonly used plasma-facing material in fusion devices [2]. Utilizing Ta as a gettering interface may enable effective control of residual HI pressure in the plasma edge, significantly improving plasma density control and mitigating energy losses associated with charge exchange, which are key challenges for small fusion reactors.

A tantalum first-wall gettering interface has been proposed for the central cell and the neutral beam injection (NBI) dump of the Wisconsin High-temperature-superconducting Axisymmetric Mirror experiment (WHAM) [3, 4]. This is a 17 T field experiment designed to advance the fusion mirror technology, validate magnetohydrodynamic interchange stabilization techniques, and benchmark computational models for the performance of the machine. WHAM utilizes high-frequency (110 GHz) electron cyclotron heating with large power density (1 MW/40 l) to achieve the breakdown plasma and build up target density prior to 25 keV NBI heating, as well as to provide additional heating to the electrons and improve overall confinement in the classical mirror regime. The experiment aims to serve as a prototype for a future $Q \sim 1$ simple axisymmetric mirror operating in the low collisionality regime.

Recent experiments have demonstrated that cold spray (CS) deposition technology holds potential for applications in fusion [5]. The cold spray deposition process offers several advantages, including a high deposition rate and efficiency, precise control over coating thickness (ranging from tens of micrometers to several millimeters), the ability to produce high-density and thick coatings, minimal oxidation, and excellent mechanical properties such as high strength and hardness [1]. Specifically, tantalum CS coatings on stainless steel (SS) substrates have been shown to maintain their physical integrity under high deuterium (D) incident fluxes and subsequent thermal annealing at 1100 K [6]. In latest years, considerable work has been devoted to characterizing the physical and mechanical properties of tantalum CS coatings, as well as their structural and morphological evolution under thermal treatments [1, 7–11].

Due to its exothermic hydrogen absorption, Ta is expected to retain more HIs than metals with endothermic hydrogen absorption [12, 13]. This effect has been experimentally demonstrated using thermal desorption spectrometry (TDS) measurements [2, 14]. However, the lack of a systematic study of D retention in Ta hinders a comprehensive interpretation of metal-hydrogen interaction mechanisms. To date, only one laboratory experiment by Novakowski *et al* [2] has addressed hydrogen retention in Ta irradiated with low-energy D ions at two distinct fluences. The authors observed that the TDS spectrum of Ta irradiated with 120 eV D ions below 470 K exhibits two discrete desorption peaks at 660 K and 760 K, while the spectrum for W shows only one desorption peak at ∼490 K, which is typical for this material [15].

The flux of charge-exchange (CX) hot neutrals on the first wall of WHAM is expected to exceed 2.5×10^{18} D m^{-2} s^{-1} in localized regions of the central cell, as a result of NBI. Exposure to high fluences of D ($>10^{21}$ D m^{-2}) leads to the formation of cavities beneath the surface, often referred to as blisters [16]. These cavities can store hydrogen and contribute to retention, as demonstrated in numerous studies on W [17–19]. Blister formation depends on factors such as incident flux, fluence, and grain orientation, resulting in uneven size and density distributions across metallic grains [17, 19]. Generally, Ta exhibits better resistance to surface deterioration (e.g. cracking and roughening) compared to W, and several studies suggest that doping W with Ta can effectively reduce blistering in W-Ta alloys [20–22].

High kinetic energy of incident particles can also cause material erosion and displacement damage in the bulk [23]. The incident kinetic energy of CX neutrals in WHAM reaches 25 keV at the tail end of their energy distribution, making damage to the first-wall material likely. High-temperature annealing is effective at reducing displacement damage in fusion materials, which may also affect their hydrogen retention properties [24]. However, the temperature of the first wall in the central cell of WHAM is expected to remain near room temperature (RT) due to the low CX energy flux ($<$6 kW m^{-2}) [3]. To establish a robust regeneration procedure for restoring the retention capacity of Ta cold spray coatings, it is essential to evaluate the temperature conditions under which HIs outgas without inducing morphological changes in the material.

Finally, there is no experimental data on the effect of the cold spray manufacturing process on HIs retention in Ta. In this study, laboratory experiments on cold spray tantalum, polycrystalline tungsten, and tantalum materials included irradiation with D ions at a kinetic energy of 95 eV, which is below the sputtering threshold for Ta (250 eV), thus avoiding the creation of additional defects at the surface and via displacement damage. To investigate the dynamics of D release from Ta and provide a comparison with the well-studied W, D retention was evaluated for incident fluences in the range of 1.6×10^{22}–3×10^{25} D m^{-2}, at fluxes of 0.9–3.5 $\times 10^{21}$ D m^{-2} s^{-1} relevant to WHAM, and at surface temperatures ranging from 400 K to 950 K. The maximum annealing temperature during thermal desorption experiments was set at 1280 K, which is close to the maximum recommended operational temperature limit for 316L SS [25].

HI retention analysis was performed in conjunction with a detailed microstructural characterization of 300 μm-thick tantalum (Ta) coatings deposited via cold spray (CS) technology onto 316L SS, a representative structural material commonly used for vacuum vessels in nuclear fusion reactors. The relatively thick Ta layer can be considered a quasi-bulk

medium for the deuterium retention study, while the SS substrate primarily serves to provide thermal conduction and mechanical integrity. This work aims to provide insights into the effects of irradiation with low-energy D plasma on retention properties in Ta cold spray coatings and polycrystalline Ta (i.e. Ta manufactured by two methods with their own unique microstructure) and to compare the results with those from reference polycrystalline W irradiated under the same conditions. The irradiation and thermal desorption parameters in this laboratory study were selected to evaluate the efficiency of the proposed Ta first-wall interface for WHAM and to provide experimental data for modeling HIs retention in Ta.

2. Experimental procedure

2.1. Sample preparation

Three sets of samples with a surface area of $10 \times 10\,\text{mm}^2$ were prepared for the experiments:

- Polycrystalline tungsten samples, identified as PCW, with a thickness of 5 mm, were procured from ALMT Corporation. They were of 99.95% purity and were recrystallized at 2073 K. PCW samples served as reference to benchmark the TDS analysis with Ta.
- Polycrystalline Ta samples, identified as PCTa, were vacuum-arc cast to a thickness of 5 mm. These were procured from Eagle Alloys Corporation. They were of 99.96% purity and annealed at 1370 K.
- Cold spray Ta samples, identified as Ta (CS), were fabricated using spherical Ta powder with an average particle size of 8 μm deposited onto 3 mm-thick 316L SS substrate coupons. This substrate thickness was chosen as the minimum required to prevent mechanical deformation under the high-velocity particle impacts of the CS process, while also limiting the overall weight of the proposed Ta first-wall interface for the WHAM.

The selection of deposition parameters was based on previous work optimizing Ta cold spray [1]. The substrates were mechanically polished using 600-grit silicon carbide paper to remove surface oxide contamination and enhance particle bonding, followed by ultrasonic cleaning in an ethanol bath prior to coating deposition. In the cold spray process, the velocity V_p of impacting particles has the most significant effect on the coating structure and physical properties [26]. In this study, nitrogen gas (N_2) was preheated to 1023 K and maintained at 3.9 ± 0.1 MPa during spraying, resulting in $V_p = 675\,\text{m s}^{-1}$. A robotic spray gun, equipped with a de Laval nozzle, and a gun translation speed of 400 mm s^{-1} was used to achieve a coating thickness of approximately 300 μm. Detailed information about the cold spray system, deposition parameters, methods for predicting V_p, and the structural and compositional stability of the produced Ta coatings under thermal treatment can be found elsewhere [6].

To reduce uncertainties related to roughness and surface oxide contamination, all samples were mechanically polished in a similar manner until a uniform mirror-like surface condition (roughness $R_a < 0.5\,\mu$m) was achieved for all samples. After polishing, the final thickness of the cold-sprayed Ta coatings was close to 200 μm.

The surface morphology of the pristine samples was examined using scanning electron microscopy (SEM). Cross-sectional observations was performed with SEM on a mechanically polished side of the Ta (CS) allowing to evaluate the thickness and morphology of the coatings.

2.2. Plasma irradiation experiments

For the plasma irradiation experiments, the samples were grouped into nine sets, each containing seven samples: one PCW, one PCTa, and five cold-sprayed Ta (CS) samples.

Two experimental campaigns were conducted. The first campaign involved four sets (a total of 28 samples) and focused on evaluating the effect of surface temperature during irradiation on D retention in the materials.

Samples in each set were simultaneously irradiated with D plasma in the linear plasma device PSI–2, located in Jülich, Germany [27]. Using a combination of heater control and water cooling capabilities of the sample stage, the samples were first outgassed at 900 K for 10 min and then cooled to the desired temperature prior to D irradiation. After placing the samples in the irradiation position in PSI–2 and initiating the plasma, the samples were biased at -100 V, resulting in a typical incident kinetic energy of D ions of ∼95 eV. A thermographic measurement system in PSI–2 monitored the surface temperature of the samples, which was maintained at 400 K, 535 K, 725 K, and 950 K during the four exposures, respectively. The maximum temperature during plasma exposure was limited to 950 K, well below the phase transformation temperatures of both tungsten and tantalum. The incident D flux, measured using a reciprocating Langmuir double probe, was $3.5 \times 10^{21}\,\text{D m}^{-2}\,\text{s}^{-1}$, with a total incident fluence of $3 \times 10^{25}\,\text{D m}^{-2}$. Immediately after exposure, the samples were cooled to RT within a few minutes to minimize deuterium diffusion and outgassing, as well as to suppress potential recovery of irradiation-induced defects in the W and Ta materials.

The second campaign focused on evaluating the effect of incident fluence on D retention in the materials, utilizing five sets (a total of 35 samples). The plasma irradiation was performed similarly to the first campaign, with the sample temperature controlled at approximately 535 K during exposure. The kinetic energy of the incident D ions and the ion flux were maintained at 95 eV and $1.6 \times 10^{21}\,\text{D m}^{-2}\,\text{s}^{-1}$, respectively. All samples in each set were simultaneously exposed to one of the following incident fluences: 1.6×10^{22}, 8.4×10^{22}, 1.0×10^{24}, 8.0×10^{24}, and $3 \times 10^{25}\,\text{D m}^{-2}$. Oxygen, the primary impurity in the PSI–2 plasma, was present at levels of approximately 0.1% [28], resulting in a negligible sputtering contribution from the plasma background for high-Z materials.

2.3. Thermal desorption experiments

After D plasma irradiation, the samples were introduced into the ultra-high vacuum CAMITER system located in Marseille, France (base pressure $< 2.3 \times 10^{-7}$ Pa) for deuterium retention quantification. Temperature calibration was carried out individually for each sample to account for differences in thermal conductivity among W, Ta and SS coated with Ta. Each sample was heated up to 1280 K with a constant temperature ramp of 1 K s^{-1} for PCW samples and 0.5 K s^{-1} for all Ta samples. Upon reaching 1280 K, the samples were held at this temperature for 10 min before being allowed to cool down to RT. A multiplexed Quadrupole Mass Spectrometer was used to simultaneously record the outgassing of HI molecules (H_2, HD, and D_2) during TDS. Time integration of the recorded deuterated molecules enabled quantification of outgassed deuterium from each sample.

The recorded TDS spectra for the cold-spray samples irradiated under identical conditions were averaged to reduce uncertainties related to differences in the thickness of the Ta coatings across the samples. Time-integrated TDS spectra allowed for retention quantification and the statistical errors were propagated accordingly.

After the TDS experiments, the surface morphology of PCW, PCTa, and Ta (CS) samples was analyzed using SEM. Cross-sectional SEM observations of surface blisters were performed on a PCW sample sectioned using the focused ion beam (FIB) technique. Prior to sectioning, protective SiO_2 and Pt layers were carefully deposited on the surface to prevent damage that can potentially occur during FIB sample preparation. Additionally, cross-sectional transmission electron microscopy (TEM) observations were performed on lamellae extracted from the Ta (CS) samples using scanning TEM at an acceleration voltage of 200 kV in a TEM FEI Titan 80-300 microscope. The Gatan Image Filter Tridiem installed in the microscope enabled Electron Energy Loss Spectroscopy (EELS) acquisition for elemental detection in the material. The energy resolution for EELS measurements was 1 eV under STEM conditions. High-angle annular dark-field (HAADF) images and EELS spectra were acquired on Ta (CS) to investigate the presence of hydrogen and oxygen in near-surface regions.

3. Results

3.1. Morphology observations of As-prepared samples prior to irradiation

Figures 1(*a*)–(*c*) show the surfaces of pristine PCW, PCTa, and Ta (CS) samples prior to D plasma exposure experiments. Grain boundaries (GBs) are faintly visible on the surface of the recrystallized PCW sample. Despite applying the same polishing procedure to the PCTa and Ta (CS) samples, some black dots (figure 1(*c*)) are observed on the surface of the Ta (CS) sample, suggesting differences in the microstructure and mechanical properties of the two samples. Cross-sectional imaging of the mechanically polished edge of the Ta (CS) sample reveals a dense coating structure resulting from strong interparticle bonding (figure 2(*a*)). During deposition, porosity at a low level (<1%) was present throughout the entire thickness (figure 2(*b*)). The black dot features observed in figure 1(*c*)) are likely manifestation of this porosity. It is important to note that cold spray parameters can be optimized to tailor the porosity level in the coatings.

3.2. Morphology observations after D irradiation and thermal desorption experiments

The surface morphology of PCW irradiated with D ions at the highest fluence of $f_{in} = 3 \times 10^{25}$ D m^{-2}, at a surface temperature of 535 K, and annealed up to 1280 K during TDS, changes significantly compared to the non-exposed W surface. Figure 1(*d*) shows that irradiation with the high fluence of D causes the appearance of surface features on PCW, ranging in size from tens of nanometers up to 0.5 μm on different tungsten grains. Cross-sectional SEM observations of the sample cut with FIB confirm that these features are blisters in the near-surface region of PCW. The size of the two blisters shown in the inset micrograph in figure 1(*d*) is approximately 320 × 110 nm. Annealing up to 1280 K during the TDS experiments did not cause the rupture of the blisters. Finally, SEM observations did not reveal blisters on the surfaces of PCW samples exposed to lower D fluence at 535 K, suggesting that either the cavities were not formed or their sizes were too small to be detected with the SEM.

Compared to tungsten, tantalum shows superior resistance to deuterium-induced surface morphology changes under the fluence and temperature conditions used in this study. SEM observations of the surface of PCTa and Ta (CS) samples irradiated with $f_{in} = 3 \times 10^{25}$ D m^{-2} at 525 K and annealed at 1280 K during TDS (figures 1(*e*) and (*f*)) show no significant morphological changes compared to the pristine surfaces (figures 1(*b*) and (*c*), respectively). Our surface observations suggest that there would be differences in irradiation-induced macro-mechanical properties between tungsten and tantalum, consistent with previous studies on deuterium-irradiated tantalum [2] and tantalum-tungsten alloys [21, 22].

Figure 3(*a*) shows a typical TEM micrograph of a Ta (CS) sample after D irradiation at $f_{in} = 3 \times 10^{25}$ D m^{-2} at 535 K and TDS up to 1280 K. A 3 nm-wide layer composed of voids is visible 5 nm below the surface within the implantation zone of 95 eV D ions, as shown in figure 3(*b*). In contrast to the blisters in the PCW sample, these voids do not impact the surface morphology and may represent the early stage of blister formation. It is worth noting that nano-voids might also be present in the near-surface region of PCTa samples. The top 5 nm layer of Ta (CS) (figures 3(*a*) and (*b*)) exhibits an amorphous structure and shows a brighter contrast than the bulk region due to a relatively lower concentration of Ta metal. EELS analysis was performed to investigate the elemental composition of the near-surface region of the sample. The spectrum acquired 10 nm below the surface (black curve in figure 4) shows a peak with the maximum intensity centered at 22.5 eV (peak A), corresponding to the

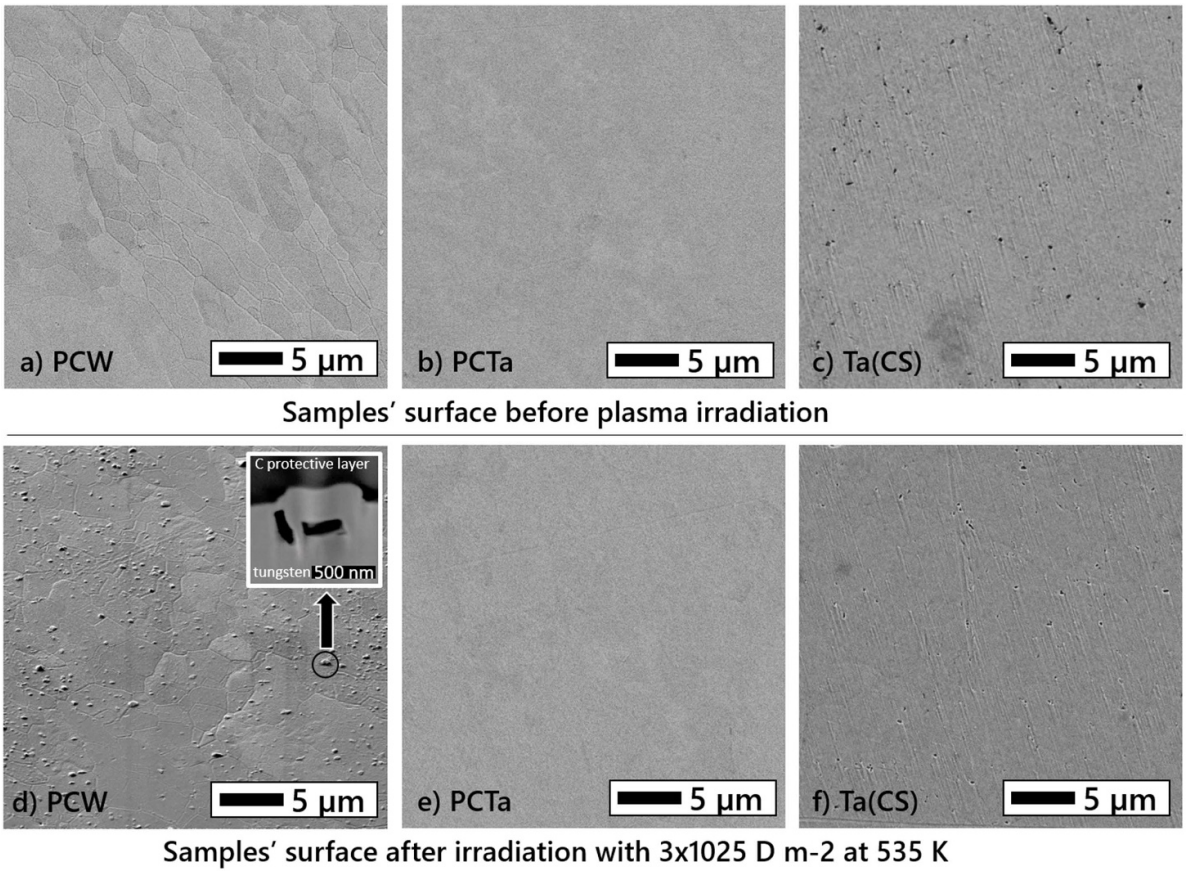

Figure 1. Typical SEM plan-view micrographs of the surface of the (*a*) PCW, (*b*) PCTa and (*c*) Ta (CS) samples in the as-prepared condition. (*d*) PCW, (*e*) PCTa and (*f*) Ta (CS) samples after irradiation with plasma. (*d*) shows blisters formed on PCW surface due to D irradiation and the inset in the figure shows the cross-sectional image of a blister.

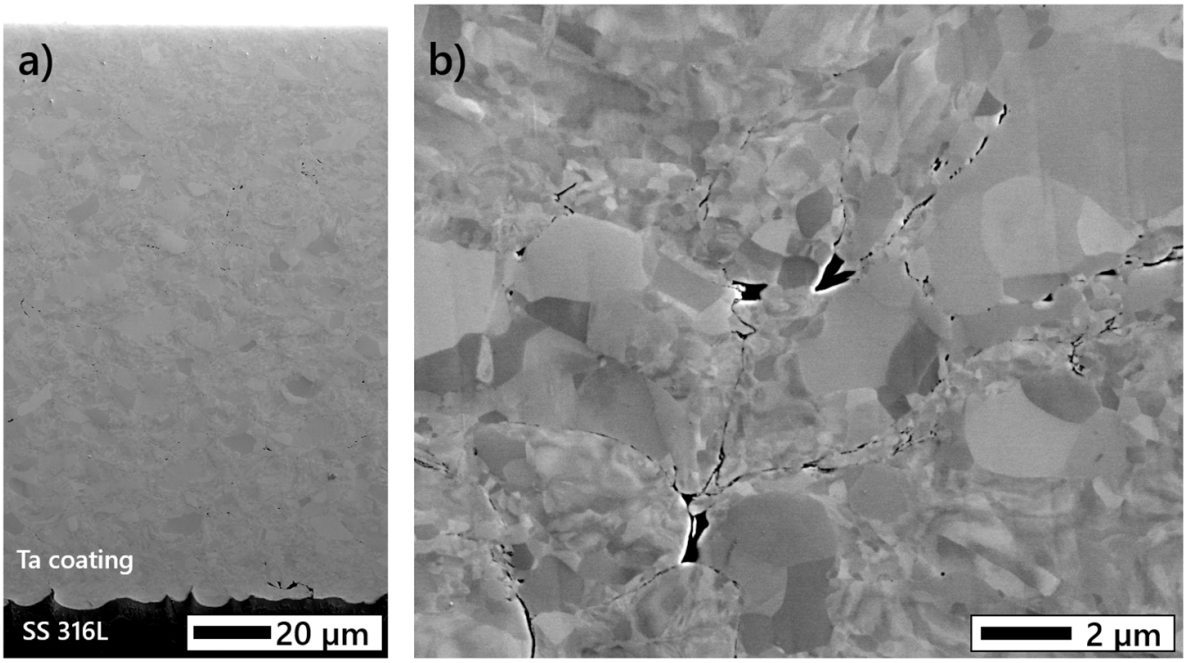

Figure 2. Typical cross-sectional SEM images of cold-sprayed Ta (CS) sample prior to D irradiation. (*a*) Low magnification image and (*b*) a high magnification image showing the microstructure of the coating.

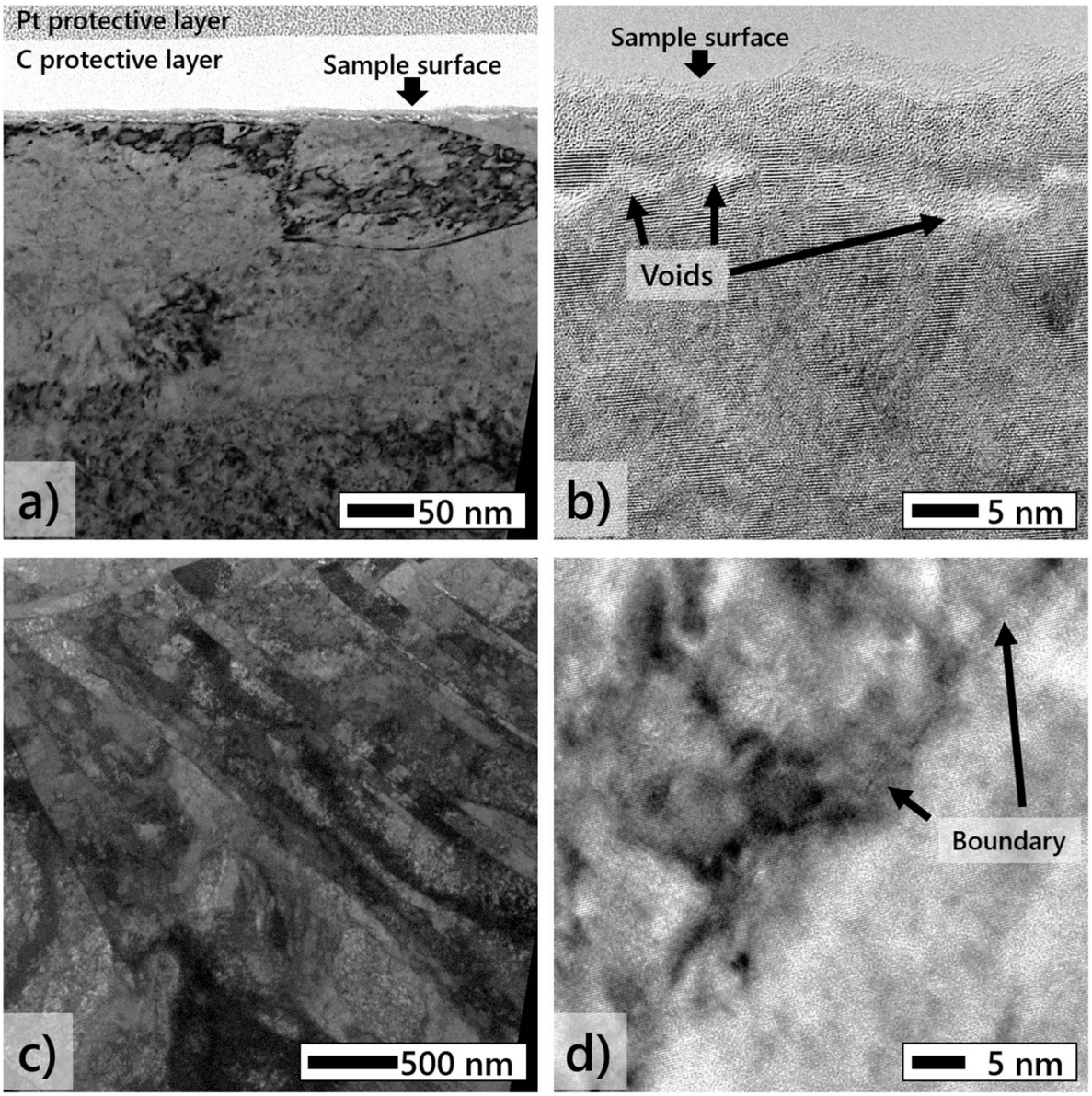

Figure 3. Cross-sectional TEM micrographs of Ta (CS) sample after D irradiation up to $f_{in} = 3 \times 10^{25}$ D m^{-2} at 535 K and thermal desorption experiments up to 1280 K. (*a*) The near-surface region and (*b*) a close-up on voids under the surface. (*c*) Bulk region of the sample 400 nm below the surface and (*d*) a close up on a boundary between two different grains.

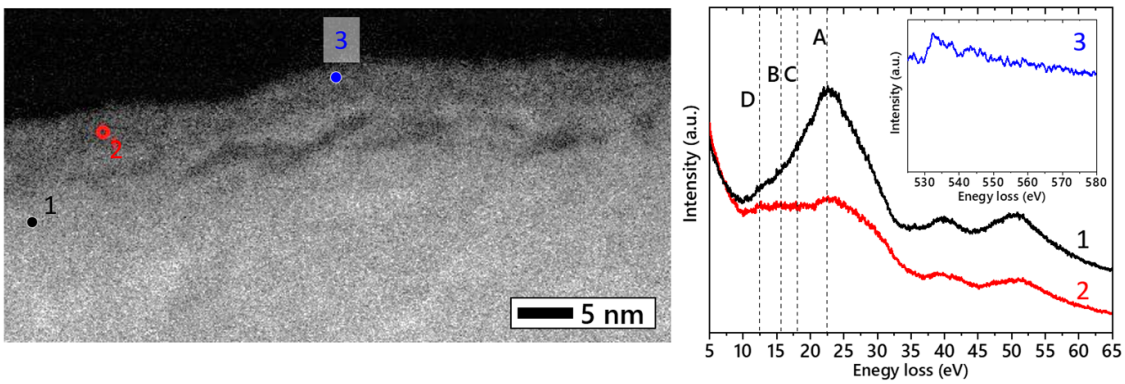

Figure 4. HAADF image (top) and Low-loss STEM-EELS measurements on the Ta (CS) sample after D irradiation and thermal desorption experiments up to 1280 K. Numbers correspond to the locations where the spectra were acquired. Inset: O K-edge spectra.

bulk plasmon excitation of metallic Ta [29]. The EELS spectrum acquired from the amorphous layer (red curve in figure 4) shows additional contributions to the bulk Ta spectrum, resulting in an increased width and shape evolution of the EELS spectra in the [5, 35] eV domain. The variation in the Ta plasmon width could be due to the high stress field and defects created by the manufacturing process and D accumulation in the near-surface region. The presence of oxygen in the top layer is confirmed by the EELS spectrum acquired close to the O K-edge (532 eV, see the blue line in figure 4). Comparison to literature results [29] allows us to conclude that the top layer on Ta (CS) samples is an amorphous $TaO_2 - x$ oxide, with peaks at (B) 15.6 eV and (C) 18 eV. The shape of the spectrum (in red in figure 4) and a small peak at (D) 12.5 eV suggest the presence of hydrogen in the amorphous layer; however, the signal is too weak to draw a definitive conclusion. Furthermore, TEM investigations highlight a high density of defects in the Ta coating, consistent with findings reported by Koivuluoto [9]. Figure 3(*a*) shows dislocation walls (dark areas) within grains, while figure 3(*c*) reveals elongated grains with high dislocation density, indicating localized high plastic deformation, all characteristic of cold spray deposition process. The grains are elongated in the direction almost perpendicular to the surface, which may play a role in D diffusion during plasma irradiation. Figure 3(*d*) shows good inter-particle bonding.

3.3. Deuterium retention as a function of incident fluence

Thermal desorption spectra for PCW, PCTa, and Ta (CS) samples exposed to various incident D fluences, f_{in}, at 535 K are presented in figure 5. In the case of PCW samples exposed to fluences below $f_{in} \leqslant 8 \times 10^{24}\,\mathrm{D\,m^{-2}}$ (figure 5(*a*)), the TDS spectra exhibit a single D desorption peak starting at 400 K and ending at 900–1000 K, with the intensity maximum at approximately 690 K. At the highest incident fluence of $f_{in} = 3 \times 10^{25}\,\mathrm{D\,m^{-2}}$, the D desorption profile undergoes significant changes. First, the width of the TDS spectra expands, and D outgassing continues up to 1150 K, which may indicate the deep diffusion of D atoms into W. Second, the intensity maximum shifts to 810 K, and the spectrum shape suggests the presence of a desorption peak at about 1000 K.

Figure 5(*b*) shows the TDS spectra of D for PCTa samples. The spectrum exhibits a flattened desorption curve for fluences below $\leqslant 8.4 \times 10^{22}\,\mathrm{D\,m^{-2}}$, while above this fluence, a sharp desorption peak appears. This contrasts with the experimental work by Novakowski *et al* [2], where D TDS spectra exhibited two discrete desorption peaks at 660 K and 760 K, with D release completing at ∼970 K. Given the similarity of irradiation conditions, this discrepancy likely arises from differences in sample preparation and annealing steps used in these two studies, which influence the nature of defects and their number density.

In figure 5(*b*), the position of the D desorption maximum for PCTa samples shifts gradually from 1150 K for $f_{in} = 1.6 \times 10^{22}\,\mathrm{D\,m^{-2}}$ to 1050 K for $f_{in} = 3 \times 10^{25}\,\mathrm{D\,m^{-2}}$. TDS experiments also reveal that D does not completely outgassed from PCTa samples even after heating up to 1280 K, indicating that a significant fraction of the implanted atoms remains trapped in the samples.

Figure 5(*c*) presents the TDS spectra for Ta (CS) as a function of incident D fluence. These spectra feature a single desorption peak up to 1280 K. The intensity maximum gradually shifts to lower temperatures with increasing fluence, from 930 K for $f_{in} = 1.6 \times 10^{22}\,\mathrm{D\,m^{-2}}$ to 860 K for $f_{in} = 3 \times 10^{25}\,\mathrm{D\,m^{-2}}$. D release from Ta (CS) samples occurs at lower temperatures, and the desorption tail decays faster compared to PCTa samples. As with PCTa, D does not completely outgas from Ta (CS) even after heating to 1280 K. The shape of the desorption tail suggests that D diffusion in the Ta (CS) plays a more important role on the isotope trapping and release than in PCTa within the range of temperatures used in this study.

The black squares in figure 6(*a*) represent the absolute number of deuterium atoms released from PCW samples as a function of incident fluence. Retention in PCW samples exposed to D at 535 K scales as $retention \propto f_{in}^{0.61}$ for fluences $f_{in} \leqslant 8.0 \times 10^{24}\,\mathrm{D\,m^{-2}}$, which is reasonably consist with the relationship $retention \propto f_{in}^{0.645}$ reported by Bisson *et al* [15] for PCW exposed to D at RT. Experimental work by Roszell *et al* [30] on polycrystalline W exposed to 500 eV D ions at 500 K reported ∼50% higher retention values than those obtained in this study, likely due to the displacement damage in their samples and the removal of a significant fraction of natural defects during at 2073 K annealing of our PCW samples prior to 95 eV/D irradiation.

Figure 6(*a*) also shows that the absolute number of D atoms released from PCTa samples (blue diamond symbols) is more than two orders of magnitude greater than D retention in PCW. Furthermore, D release from tantalum exhibits two distinct regimes. The first 'high-trapping' regime occurs at low fluences ($f_{in} \leqslant 2.8 \times 10^{22}\,\mathrm{D\,m^{-2}}$) and is characterized by D retention exceeding the percentage of non-reflected ions predicted using the SRIM code for the irradiation conditions used in this study (dashed blue line in figure 6(*a*). The second 'low-trapping' regime occurs at high fluences ($f_{in} > 2.8 \times 10^{22}\,\mathrm{D\,m^{-2}}$) and is characterized by a decrease in D retention below the theoretical retention maximum predicted by SRIM. It is important to note that SRIM calculations account only for compositional changes due to the spatial distribution of target atoms deposited in collision cascades in pure W and Ta materials. Also, these calculations do not consider the effects of temperature during D irradiation. However, they provide an estimate of the theoretical upper limit of reflected and directly implanted D ions in pure W and Ta.

The red dots in figure 6(*a*) represent the absolute number of D atoms released from cold-spray tantalum samples (Ta (CS)), which is approximately 3.5 times greater than that of PCTa. D release from Ta (CS) samples as a function of incident fluence follows the same trend as observed for PCTa samples, with 'high-trapping' and 'low-trapping' regimes clearly evident.

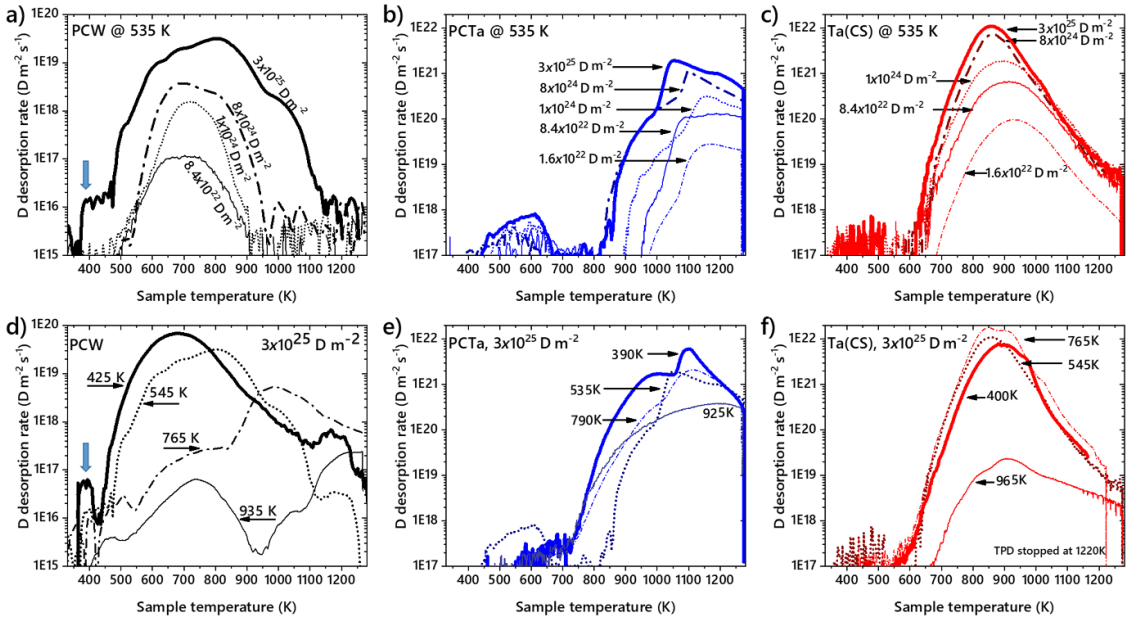

Figure 5. Thermal desorption rate for PCW, PCTa and cold spray tantalum Ta (CS) samples: (*a*)–(*c*) as a function of the incident fluence at ∼535 K and (*d*)–(*f*) as a function of the surface temperature during D irradiation up to 3×10^{25} D m^{-2}. The blue arrows in (*a*) and (*d*) indicate the desorption peak originating from a poor temperature control.

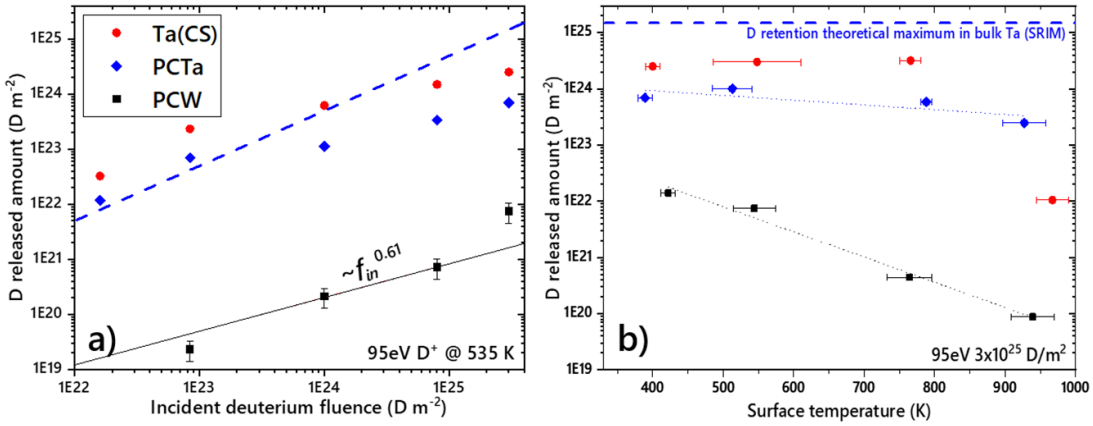

Figure 6. TDS results for PCW, PCTa and cold spray tantalum Ta (CS) samples. Quantity of outgassed D as a function (*a*) of incident fluence and (*b*) of surface temperature during the D plasma exposure. Blue dashed line represents the SRIM implantation probability for impinging 95 eV D ions on tantalum. Dotted lines are provided for clearer visualization.

3.4. Deuterium retention as a function of surface temperature

Figures 5(*d*)–(*f*) show the evolution of the D desorption rate for PCW, PCTa, and Ta (CS) samples, respectively, as a function of the surface temperature (T_{impl}) during D irradiation up to a fluence of 3×10^{25} D m^{-2}. For PCW (figure 5(*d*)), an increase in T_{impl} from 425 K to 935 K gradually shifts the position of the lower-temperature desorption peak from 685 K to 740 K and reduces its intensity by more than three orders of magnitude. This indicates D release from traps associated with this desorption peak. Additionally, the shift of the desorption maxima from 685 K to at least 1250 K, coupled with the incomplete deuterium release even upon reaching 1280 K during TDS measurements, highlights D migration and trapping deep within the bulk of PCW at elevated T_{impl}.

For PCTa (figure 5(*e*)), the TDS spectra exhibit a sharp desorption peak in the temperature range of 390–790 K. At $T_{\mathrm{impl}} = 925$ K, the desorption spectrum flattens, and the TDS intensity maximum decreases by an order of magnitude, suggesting that D is present to a lesser extent in associated traps and likely diffuses deeper into the bulk during irradiation at elevated temperatures.

In the case of Ta (CS) (figure 5(*f*)), the position of the desorption maxima remains independent of the surface temperature during irradiation. However, at $T_{\mathrm{impl}} = 965$ K, a drastic decrease in its intensity is observed, indicating that

D retention is significantly reduced in the coatings at this temperature.

Figure 6(*b*) summarizes the retention measurements for PCW, PCTa, and Ta (CS) samples as a function of T_{impl} during D implantation. For PCW samples, D retention decreases by two orders of magnitude as T_{impl} increases from 400 K to 925 K, consistent with previous studies [30, 31]. For PCTa and Ta (CS) samples, the amount of outgassed D during TDS measurements up to 1280 K remains nearly constant from 400 K to 800 K, constituting approximately 2.3% and 8.4% of f_{in}, respectively. However, at $T_{\mathrm{impl}} = 925$ K, D retention decreases to 0.83% of the incident fluence for PCTa and drops sharply to 0.04% for Ta (CS).

4. Discussion

To understand the trapping mechanisms for D in the materials, we use Redhead's methodology to determine the activation energy for desorption. The D desorption rate from a surface can be expressed as [32]:

$$-\frac{\mathrm{d}\Theta}{\mathrm{d}T} = \frac{\nu_0}{\beta}\Theta^m \exp\left(-\frac{E_d}{k_B T}\right), \tag{1}$$

where $\Theta = \frac{c_{\mathrm{surface}}}{n_{\mathrm{surface}}}$ is the surface coverage (c_{surface} is the concentration of D atoms on the surface and n_{surface} is the concentration of available adsorption sites), $T(t) = T_0 + \beta t$ is the surface temperature at a given time t for a heating rate of β K s^{-1}, ν_0 is the attempt frequency (assumed 10^{13} s^{-1}), m is the order of desorption, E_d is the activation energy for desorption (detrapping energy), and k_B is the Boltzmann constant.

Our experiments on PCW reveal that the temperature position of the desorption maximum remains constant at low fluences but shifts to higher temperatures for the highest fluence of $f_{in} = 3 \times 10^{25}$ D m^{-2} (figure 5). Bisson *et al* [15] demonstrated that the shift of the main desorption peak to higher temperatures with increasing fluence is associated with D diffusion deeper into the bulk of tungsten. This behavior is consistent with first-order desorption kinetics, where the position of the desorption peak is independent of Θ. Solving equation (1) for $m = 1$ allows the evaluation of the activation energy E_d:

$$\frac{\beta}{k_B T_m^2} = \frac{\nu_0}{E_d}\exp\left(-\frac{E_d}{k_B T_m}\right), \tag{2}$$

where T_m is the temperature position of the desorption peak. For $T_m = 690$ K and $\beta = 1$ K s^{-1}, $E_d = 2.0$ eV for PCW. In general, this activation energy is consistent with D detrapping from GBs [33, 34] and voids [35, 36], which is expected since vacancies should have disappeared in PCW after annealing at 2073 K prior to D irradiation [37]. At the highest fluence of 3×10^{25} D m^{-2}, blister formation is observed in the near-surface of PCW. Studies by Liu *et al* [19] suggest that retention is primarily associated with D release from dislocation- and vacancy-type defects created around blisters during high-fluence irradiation, rather than from D_2 molecules trapped in blister cavities. Similarly, Roszell *et al* [30] identified a trap energy of 2.1 eV for D trapped in nano-voids formed during implantation at temperatures above 450 K.

Unlike other studies [18, 19], no sudden excursions of D signals in the low-temperature region of the TDS spectra (<750 K) were observed, indicating that blisters did not rupture during our thermal desorption experiments (figure 5(*a*)). The significantly higher D retention for PCW at $f_{in} = 3 \times 10^{25}$ D m^{-2} compared to lower fluences is consistent with $retention \propto f_{in}^{0.61}$ (figure 6(*a*)). At low fluences, D is primarily trapped at GBs and diffuses into the bulk, as evidenced by the desorption profile ending at 900–1000 K. As fluence increases, nano-voids form in the near-surface regions, contributing to D trapping and resulting in a desorption peak at ∼810 K. For the highest fluence, some voids grow into surface blisters, acting as stronger traps at ∼1000 K. Long plasma exposure times and elevated T_{impl} also allow D to diffuse deeper into the bulk, shifting the desorption maximum to higher temperatures during TDS.

The desorption experiments with PCTa and Ta (CS) samples show a shift in the desorption peak maximum toward lower temperatures with increasing fluence, indicative of second-order desorption kinetics. Here, the recombination of D atoms on the surface is the rate-limiting process. At low fluences, $\Theta < 1$, the desorption peak maximum shifts to lower temperatures with increasing fluence until saturation ($\Theta = 1$) is reached. At higher fluences, D diffuses deeper into the bulk, which can counteract this temperature shift. Figure 5(*c*) shows that the desorption peak starts to stall only at the highest fluence level investigated in this study. Differentiating equation (1) for $m = 2$ yields the activation energy for desorption:

$$\frac{\beta}{k_B T_m^2} = 2\Theta\frac{\nu_0}{E_d}\exp\left(-\frac{E_d}{k_B T_m}\right). \tag{3}$$

Assuming $\Theta = 1$ for $f_{in} = 3 \times 10^{25}$ D m^{-2}, we evaluate $E_d = 3.15$ eV for PCTa ($T_m = 1050$ K, $\beta = 0.5$ K s^{-1}) and $E_d = 2.56$ eV for Ta (CS) ($T_m = 860$ K, $\beta = 0.5$ K s^{-1}). These values are higher than those reported in [2], warranting further modeling to explore the origins of this discrepancy.

Our results confirm the high HI trapping efficiency of Ta compared to W. The D desorption spectra intensity is two orders of magnitude higher for PCTa than for PCW, indicating a greater density of D trapping sites in Ta. High hydrogen diffusion rates in Ta may also promote hydride formation [38–40], similar to, for example, titanium hydrides [41]. Our previous work on Ta irradiated at 3×10^{25} D m^{-2} supports the formation of tantalum deuteride [6]. Subsequently, embedding of D in Ta in the form of chemically stable compound D_xTa increases D inventory in the material. Further studies are needed to directly confirm the presence of deuterides in our samples.

The observed 'high-trapping' and 'low-trapping' regimes (figure 6(*a*)) likely result from Ta's exothermic hydrogen absorption properties. Due to the high energy of traps, the majority of deuterium implanted during irradiation at low fluences and surface temperature below 925 K remains retained

in Ta while only a small fraction of the atoms may recombine at the surface. Additionally,the metal absorbs D from the plasma before and after the bias voltage is applied to the samples. With increase of the exposure time, nano-voids are created and the sub-surface trapping sites saturated with D act as a diffusion barrier, limiting D inventory.

It is important to note that, under our experimental conditions, thermal effects during plasma exposure and TDS do not induce compositional or structural changes in the cold-sprayed coatings as reported in previous work [6]. Thus, we suggest that the differences in D trapping between PCTa and Ta (CS) samples (figures 5 and 6) may be attributed to microstructural differences. The cold-spray manufacturing process introduces numerous defects (e.g. vacancy complexes, dislocations, grain and sub-GBs, and pores down to nanometers scale) [42, 43], as evidenced by SEM and TEM examinations in our sample (figures 2 and 3). Since the Ta (CS) coatings were only outgassed at 900 K prior to plasma exposures and the majority of the defects with low de-trappping energy for D are expected to remain in the samples. D release from these traps in Ta (CS) occurs at lower temperature compared to PCTa. Defect annihilation during plasma exposures at elevated temperature of $T_{\mathrm{impl}} = 965$ K would explain the significant reduction of D retention in the coatings. In contrast, annealing of PCTa at 1370 K before D implantation likely brings down the density of single vacancies and vacancy clusters, resulting in overall lower retention at $T_{\mathrm{impl}} < 900$ K and D trapping on traps with high de-trap energy, compared to Ta (CS) (figure 6). The presence of inter-particle boundaries and microscale cavities in Ta (CS) would promote D diffusion, providing D atoms access to a larger surface area deeper in the material and facilitating population of the traps. These channels also facilitate D release during TDS. The lower desorption temperature enhances the functionality of Ta (CS) coatings as a gettering first-wall interface for WHAM, ensuring structural integrity below the operational temperature limit of 316L SS [25] while enabling effective D release.

5. Conclusions

Deuterium retention in tantalum cold spray coatings has been studied using TDS up to temperatures of 1280 K and compared to deuterium retention in polycrystalline tungsten and polycrystalline tantalum. Pure Ta coatings were deposited on 316L stainless-steel substrates using spherical powder feedstock under the impact velocity of approximately 675 m s^{-1}.

The materials were irradiated with deuterium ions with kinetic energy of 95 eV (3×10^{25} D m^{-2} at 1053–1073 K) at the flux 1.6–3.5 $\times 10^{21}$ D m^{-2} s^{-1}. For implantations at incident fluence ranging between 1.6×10^{22}–3×10^{25} D m^{-2} and constant surface temperature of 535 K, deuterium retention in tantalum coatings was, in general, 3.5 times greater than in polycrystalline Ta and more than 2 orders of magnitude greater than in polycrystalline W. Deuterium trapping exceeded the theoretical retention maximum predicted by SRIM for tantalum for fluences below 8.4×10^{22} D m^{-2} highlighting the exothermic hydrogen absorption property of the material while a saturation of trapping sites for D was evidenced at higher fluences.

Deuterium retention in polycrystalline and cold spray Ta appeared to be independent of substrate temperature over the range of 400–800 K and at 925 K dropped by a factor of 3 in the case of polycrystalline Ta and over two orders of magnitude in the case of cold spray Ta coatings. Thermo-desorption results revealed the 2nd order desorption kinetics in case of tantalum, highlighting the difference to the known first order desorption kinetics of deuterium from tungsten. The calculated activation energies for desorption were: 2.0 eV for for polycrystalline W, 3.15 eV for polycrystalline Ta and 2.56 eV for cold spray Ta coatings.

Cross-sectional SEM observations revealed blisters on the surface of tungsten irradiated at the highest deuterium fluence of 3×10^{25} D m^{-2} at temperature up to 725 K, which did not rupture after thermal desorption experiments at 1280 K. Surface and cross-sectional observations of polycrystalline Ta and cold spray Ta coatings highlighted the superior resistance of these materials to irradiation-induced morphological evolution compared to tungsten. Deuterium irradiation resulted in nano-void formation below the natural oxide layer on the surface of the cold spray tantalum coatings. The coatings themselves are characterized by a high density of defects and dislocation walls, grain and sub-GBs, interparticle boundaries, and porosity down to nanometric scales. This large number of internal interfaces likely promotes deuterium diffusion in the cold spray coatings, and associated access to a larger number of trapping sites resulting in an enhanced deuterium inventory compared to polycrystalline tantalum.

In future work we will focus on experimental validation of the tantalum first-wall interface subjected to both, low-temperature gas and 25 keV neutral beam irradiation in WHAM. Numerical simulations of the experimental deuterium thermal desorption spectra will help to identify the differences in fundamental mechanisms of HIs migration and retention in tungsten and tantalum.

Acknowledgments

The information, data, or work presented herein was funded in part by the Advanced Research Projects Agency-Energy (ARPA-E), U.S. Department of Energy, under Award Number DE-AR0001258. The views and opinions of authors expressed herein do not necessarily state or reflect those of the United States Government or any agency thereof. The authors gratefully acknowledge the use of facilities and instrumentation at the UW-Madison Wisconsin Centers for Nanoscale Technology (wcnt.wisc.edu) partially supported by the NSF through the University of Wisconsin Materials Research Science and Engineering Center (DMR-1720415). We also acknowledge Janith Wanni and Buzz Rankouhi from Prof. Thoma's group at the University of

Wisconsin-Madison for their help with cross-sectional scanning electron microscopy observations on one of the tungsten samples.

References

[1] Kumar S., Vidyasagar V., Jyothirmayi A. and Joshi S.V. 2016 *J. Therm. Spray Technol.* **25** 745–56
[2] Novakowski T., Sundaram A., Tripathi J., Gonderman S. and Hassanein A. 2018 *J. Nucl. Mater.* **Z504** 1–7
[3] Endrizzi D. *et al* 2023 *J. Plasma Phys.* **89** 975890501
[4] Forest C. *et al* 2023 *J. Plasma Phys.* **90** 975900101
[5] Neu R., Maier H., Böswirth B., Elgeti S., Greuner H., Hunger K., Kondas J. and von Müller A. 2023 *Nucl. Mater. Energy* **34** 101343
[6] Ialovega M. *et al* 2023 *Phys. Scr.* **98** 115611
[7] Jafarlou D.M., Sousa B.C., Gleason M.A., Ferguson G., Nardi A.T., Cote D.L. and Grosse I.R. 2021 *Addit. Manuf.* **47** 102243
[8] Koivuluoto H., Näkki J. and Vuoristo P. 2009 *J. Therm. Spray Technol.* **18** 75–82
[9] Koivuluoto H., Honkanen M. and Vuoristo P. 2010 *Surf. Coat. Technol.* **204** 2353–61
[10] Delloro F., Jeandin M., Jeulin D., Proudhon H., Faessel M., Bianchi L., Meillot E. and Helfen L. 2017 *J. Therm. Spray Technol.* **26** 1838–50
[11] Bailly O., Laguionie T., Bianchi L., Vardelle M. and Vardelle A. 2012 *Proc. Int. Thermal Spray Conf.*
[12] Haussalo P., Keinonen J., Jäske U. and Sievinen J. 1994 *J. Appl. Phys.* **75** 7770–3
[13] Takagi I., Nagaoka S., Shirai K., Moritani K. and Moriyama H. 2003 *Phys. Scr.* **2003** 121
[14] Hirai T., Rubel M., Philips V., Huber A., Tanabe T., Wada M., Ohgo T., Pospieszczyk A., Sergienko G. and Wienhold P. 2003 *Phys. Scr.* **2003** 59
[15] Bisson R., Markelj S., Mourey O., Ghiorghiu F., Achkasov K., Layet J.-M., Roubin P., Cartry G., Grisolia C. and Angot T. 2015 *J. Nucl. Mater.* **467** 432–8
[16] Dias M., Mateus R., Catarino N., Franco N., Nunes D., Correia J., Carvalho P., Hanada K., Sârbu C. and Alves E. 2013 *J. Nucl. Mater.* **442** 69–74
[17] Wang W., Roth J., Lindig S. and Wu C. 2001 *J. Nucl. Mater.* **299** 124–31
[18] Shu W., Kawasuso A. and Yamanishi T. 2009 *J. Nucl. Mater.* **386–388** 356–9
[19] Liu M. *et al* 2020 *Nucl. Fusion* **60** 126034
[20] Wirtz M., Linke J., Pintsuk G., Singheiser L. and Uytdenhouwen I. 2011 *Phys. Scr.* **2011** 014058
[21] Zayachuk Y., 't Hoen M., van Emmichoven P.A.Z., Terentyev D., Uytdenhouwen I. and van Oost G. 2013 *Nucl. Fusion* **53** 013013
[22] Zhou H., Jiao Q., Liu R., Liu C., Yan S., Chen X., Feng G., Zhang H. and Li L. 2021 *J. Phys.: Conf. Ser.* **1802** 022106
[23] Yoshida N. and Hirooka Y. 1998 *J. Nucl. Mater.* **258–263** 173–82
[24] Lhuillier P.E., Barthe M.F., Desgardin P., Egger W. and Sperr P. 2009 *Phys. Status Solidi c* **6** 2329–32
[25] Setyowati V.A., Suheni, Widodo E.W.R. and Hermanto S.A. 2019 *IOP Conf. Ser.: Mater. Sci. Eng.* **462** 012012
[26] Dykhuizen R.C. and Smith M.F. 1998 *J. Therm. Spray Technol.* **7** 205–12
[27] Kreter A., Brandt C., Huber A., Kraus S., Möller S., Reinhart M., Schweer B., Sergienko G. and Unterberg B. 2015 *Fusion Sci. Technol.* **68** 8–14
[28] Schmitz J. *et al* 2018 *Nucl. Mater. Energy* **15** 220–5
[29] Park G.-S. *et al* 2013 *Nat. Commun.* **4** 2382
[30] Roszell J., Davis J. and Haasz A. 2012 *J. Nucl. Mater.* **429** 48–54
[31] Haasz A., Davis J., Poon M. and Macaulay-Newcombe R. 1998 *J. Nucl. Mater.* **258–263** 889–95
[32] Redhead P. 1962 *Vacuum* **12** 203–11
[33] Li X.C., Shu X., Liu Y.N., Gao F. and Lu G.H. 2011 *J. Nucl. Mater.* **408** 12–17
[34] Yu Y., Shu X., Liu Y.-N. and Lu G.-H. 2014 *J. Nucl. Mater.* **455** 91–95
[35] Poon M., Haasz A. and Davis J. 2008 *J. Nucl. Mater.* **374** 390–402
[36] Hou J., Kong X.-S., Wu X., Song J. and Liu C.S. 2019 *Nat. Mater.* **18** 833–9
[37] Bernard E. *et al* 2019 *Nucl. Mater. Energy* **19** 403–10
[38] Lecocq P. and Wert C. 1975 *Thin Solid Films* **25** 77–84
[39] Park K.-T., Park J.-H., Yoon J.-H., Lee J.-E. and Park I.-K. 2017 *Int. J. Refract. Met. Hard Mater.* **65** 83–87
[40] Lee J.-E., Yoon J.-H., Lee C.-G., Park J.-H. and Park I.-K. 2019 *Int. J. Refract. Met. Hard Mater.* **79** 90–94
[41] Tsuchiya B., Oku M., Sahara R., Nagata S., Shikama T. and Kawazoe Y. 2008 *J. Surf. Anal.* **14** 424–7 (available at: https://api.semanticscholar.org/CorpusID:55709905)
[42] Kim Y.-K., Kim H.-J. and Lee K.-A. 2023 *J. Mater. Res. Technol.* **23** 5698–709
[43] Wei J., Aghasibeig M., Lyu T., Liu Z., Chen H., Irissou E. and Zou Y. 2024 *Surf. Coat. Technol.* **480** 130621